

COMPARISON OF DISPERSION CHARACTERISTICS OF HOLLOW-CORE PHOTONIC CRYSTAL FIBERS FILLED WITH AROMATIC COMPOUNDS

Thuy Nguyen Thi^{1*}, Trong Dang Van¹, Duc Hoang Trong¹, Tran Tran Bao Le¹, Bao Le Xuan²,
Vu Tran Quoc³, Ngoc Vo Thi Minh⁴, Lanh Chu Van⁵

¹ University of Education, Hue University, 34 Le Loi St., Hue, Vietnam

² Phan Boi Chau High School for The Gifted, 119 Le Hong Phong St., Vinh City, Vietnam

³ Thu Khoa Nghia High School for The Gifted, Chau Doc City, An Giang, Vietnam

⁴ Huynh Thuc Khang High School, Gia Lai, Vietnam

⁵ Vinh University, 182 Le Duan St., Vinh City, Vietnam

* Corresponding author: Thuy Nguyen Thi <ntthuy@hueuni.edu.vn>

(Received: 28 April 2021; Accepted: 7 July 2021)

Abstract. In this paper, hollow-core photonic crystal fibers (PCFs) infiltrated with benzene and nitrobenzene are designed and investigated. Their dispersion characteristics are numerically simulated. The results show that using the aromatic-compounds-filled hollow core of PCFs makes dispersion curves flat. In addition, the dispersion curves approach the zero-dispersion line closer than previously published dispersion curves of PCFs with toluene, thus significantly improving the supercontinuum generation to create the ultra-flat spectrum expansion.

Keywords: photonic crystal fibers (PCFs), aromatic compounds, benzene, nitrobenzene, flat dispersion

1 Introduction

The first photonic crystal fiber (PCF) was designed and investigated by Russell in 1996 [1]. Since then, it has attracted specialists' attention worldwide in studying and improving PCFs with different configurations. The PCF's nonlinear properties are beneficial in diverse applications because of their advantages compared with conventional optical fibers [2-8]. The properties of PCFs, deciding their application are effective refractive index [9-11], guiding mechanism of light in photonic crystal fibers [12], effective mode area [13, 14], dispersion [15-20], and confinement loss [21-23]. Depending on the applications, the properties of PCF can be profoundly changed by infiltrating air holes with optical liquids. In recent years, much work on the PCFs infiltrated with liquids has exhibited exciting characteristics, such as different refractive indices and higher

nonlinearity on the cladding or in the core of photonic crystal fiber as designing a dual-core PCF coupler [24], D-glucose sensor with PCFs [25], controlling dispersion engineering of PCFs [26], and liquid-filled simplified hollow-core PCFs [27]. Infiltration with liquids in the core of PCFs has a high loss limitation, but it has higher nonlinearity because the fundamental mode is well confined in the core [28]. This property makes PCFs a suitable medium for a supercontinuum generation [29-31]. The solid-core and hollow-core PCFs differ in their structure, with silica in the centre of the core for the solid core and a liquid for the hollow core. It means that the light transmission in hollow-core PCFs is the same as in solid-core PCFs, while the principle of total reflection remains [5]. It has already been demonstrated that a broad supercontinuum generation is possible by using

liquids, such as carbon tetrachloride [32, 33], toluene [32, 33], and carbon disulfide [32-34].

The nonlinear refractive index of nitrobenzene ($685 \times 10^{-20} \text{ m}^2/\text{W}$ at $1.064 \mu\text{m}$ [32, 33]) is higher than that of toluene ($160 \times 10^{-20} \text{ m}^2/\text{W}$ at $1.064 \mu\text{m}$ [32, 33]). This improvement gives us an idea to design a PCF with a hollow core infiltrated with benzene and nitrobenzene. These materials are expected to improve the efficiency of supercontinuum generation.

The PCFs with a hollow core infiltrated with toluene were designed and investigated in detail by Chu Van et al. [28]. Two optimal structures with a lattice constant of $2 \mu\text{m}$ and filling factors 0.3 and 0.35 were analyzed and discussed for a supercontinuum generation. Because of the intense light absorption of toluene and the inadequacy of nonlinear refractive index, there were some limitations in the PCFs infiltrated with toluene, such as the high confinement loss (0.4 dB/cm) and the large effective mode area.

To overcome these limitations, in this paper, we used benzene and nitrobenzene as liquids to fill the hollow core of PCFs. The properties were simulated, discussed, and compared with those of the PCFs infiltrated with toluene. The optimized structures were suggested to use in supercontinuum generation.

2 PCF's numerical model

The Lumerical Mode Solutions software was used to design the structure of PCFs. The geometrical

structure diagram of PCFs with a hollow core infiltrated with aromatic compounds is shown in Fig. 1. The base material is fused silica glass, and the hollow core is infiltrated with benzene (PCF-B), nitrobenzene (PCF-N), and toluene (PCF-T) [28]. The photonic shell consists of eight gas-hole rings with a diameter d , arranged in an equilateral hexagon with a lattice constant Λ . The diameter of the core is determined from the formula $D_c = 2\Lambda - 1.1d$. The sheath's linear filling factor is defined as $f = d / \Lambda$. In numerical simulation, the lattice constants were chosen from 1.0 to $2.5 \mu\text{m}$, while the filling factors vary from 0.3 to 0.8 .

The parameters are presented in Table 1. The smallest core ($D_c = 1.12 \mu\text{m}$) is reached when $\Lambda = 1.0 \mu\text{m}$ and $f = 0.8$, while the largest ($D_c = 4.18 \mu\text{m}$) is obtained when $\Lambda = 2.5 \mu\text{m}$ and $f = 0.3$. The chosen range of parameters corresponds to the technological requirements of the stacking method commonly used to develop PCFs.

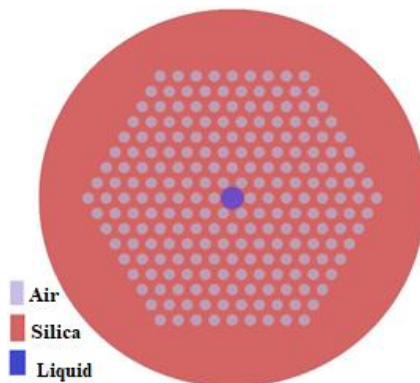


Fig. 1. Geometrical structure of PCFs with hollow core infiltrated with aromatic compounds

Table 1. Simulation parameters for PCF structure design

		$\Lambda = 1.0 \mu\text{m}$										
f		0.3	0.35	0.4	0.45	0.5	0.55	0.6	0.65	0.7	0.75	0.8
d		0.3	0.35	0.4	0.45	0.5	0.55	0.6	0.65	0.7	0.75	0.8

D_c	1.67	1.615	1.56	1.51	1.45	1.40	1.34	1.29	1.23	1.18	1.12
$\Lambda = 1.5 \mu\text{m}$											
f	0.3	0.35	0.4	0.45	0.48	0.5	0.55	0.6	0.65	0.7	0.75
d	0.45	0.53	0.6	0.68	0.72	0.75	0.83	0.9	0.98	1.05	1.13
D_c	2.51	2.42	2.34	2.26	2.21	2.18	2.10	2.01	1.93	1.85	1.76
$\Lambda = 2.0 \mu\text{m}$											
f	0.3	0.35	0.4	0.45	0.48	0.5	0.55	0.6	0.65	0.7	0.75
d	0.6	0.7	0.8	0.9	0.96	1	1.1	1.2	1.3	1.4	1.5
D_c	3.34	3.23	3.12	3.01	2.94	2.9	2.79	2.68	2.57	2.46	2.35
$\Lambda = 2.5 \mu\text{m}$											
f	0.3	0.35	0.4	0.45	0.5	0.55	0.6	0.65	0.7	0.75	0.8
d	0.75	0.88	1	1.13	1.25	1.38	1.5	1.63	1.75	1.88	2
D_c	4.18	4.04	3.9	3.76	3.63	3.49	3.35	3.21	3.08	2.94	2.8

3 Results and discussion

3.1 Dispersion characteristics of PCFs

Fig. 2 to Fig. 5 present the dependence of dispersion of PCFs on various values of f and Λ . We can see that with the same structural parameters, the dispersion curves of PCF-B, PCF-N, PCF-T [28] change with wavelength and have a similar shape.

In Fig. 2 ($\Lambda = 1.0 \mu\text{m}$), the slope of the dispersion curves of PCF-B, PCF-N, PCF-T is high. When f varies from 0.7 to 0.8, some dispersion curves have two zero-dispersion wavelengths (ZDW). For the remaining values of f , the normal dispersion curves (negative dispersion values) are observed.

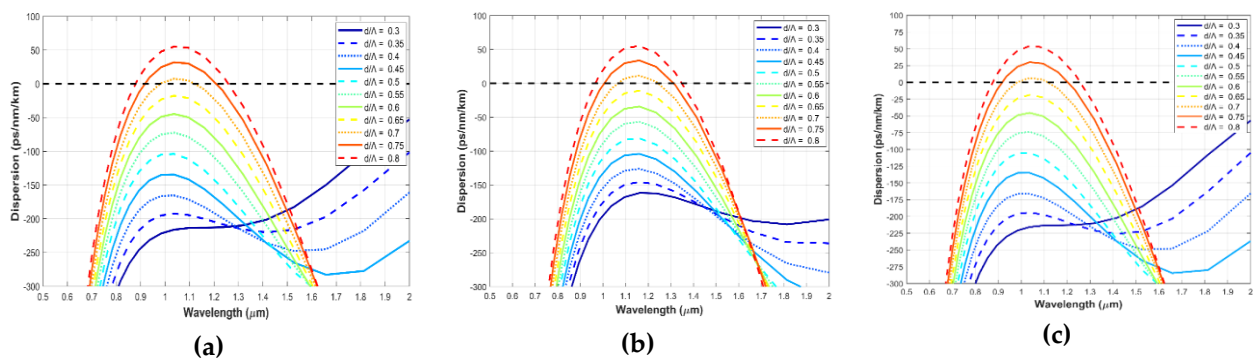


Fig. 2. Dispersion as a function of wavelength of the fiber with various f when $\Lambda = 1.0 \mu\text{m}$, a) Benzene; b) Nitrobenzen; c) Toluene

The dispersion curves of the fiber with various f when $\Lambda = 1.5 \mu\text{m}$ are shown in Fig. 3. The curves of PCF-B, PCF-N, and PCF-T in Fig. 3 are flatter than those in Fig. 2. The fibers have

dispersion curves with two ZDW values, or they closer approach the zero-dispersion curve when the filling factor f is from 0.5 to 0.8. The remaining structures give normal dispersion.

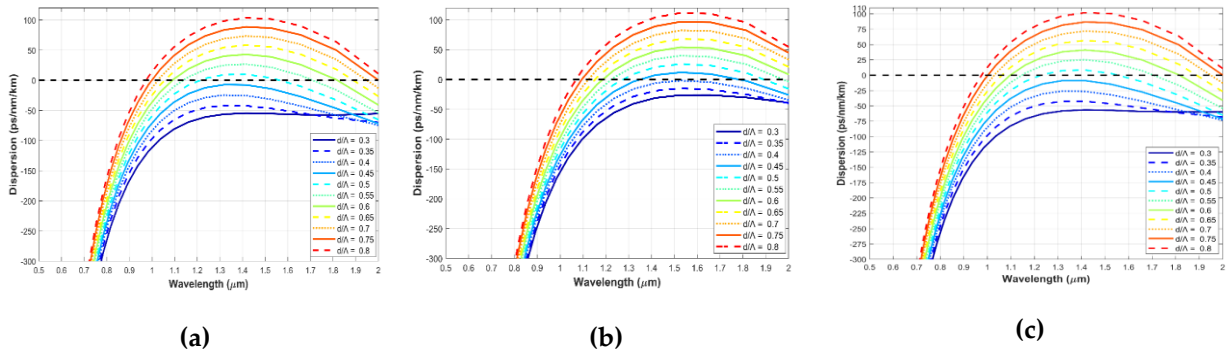


Fig. 3. Chromatic dispersion as a function of wavelength of the fiber with various f when $\Lambda = 1.5 \mu\text{m}$, a) Benzene; b) Nitrobenzen; c) Toluene

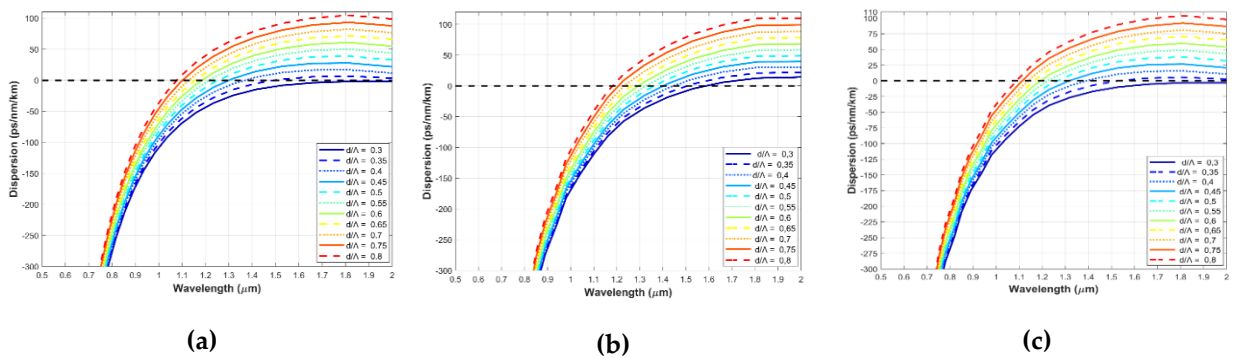


Fig. 4. Chromatic dispersion as a function of wavelength of the fiber with various f when $\Lambda = 2.0 \mu\text{m}$, a) Benzene; b) Nitrobenzen; c) Toluene

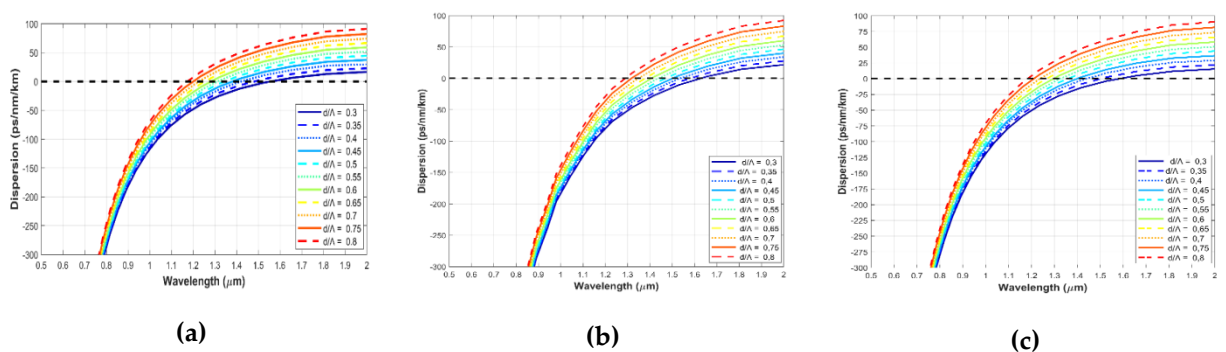


Fig. 5. Chromatic dispersion as a function of wavelength of the fiber with various f when $\Lambda = 2.5 \mu\text{m}$, a) Benzene; b) Nitrobenzen; c) Toluene

When the lattice constants are 2 and 2.5 μm (Figs. 4 and 5), the dispersion curves of the PCF-B, PCF-N, and PCF-T are flatter than those with the lattice constant 1.5 μm . These curves are very flat in the wavelength range of 0.9–2.0 μm . All dispersion curves also cut the zero-dispersion line, indicating that the ZDW values exist. This result is entirely consistent with that of Chu Van et al. [28]. In these structures, the slope and flatness of the dispersion curves are strongly dependent on the wavelength, the filling factor f , and the lattice constant Λ . This is explained by the dependence of the dispersion on the effective refractive index and wavelength according to the

$$D = -\frac{\lambda}{c} \frac{d^2 \text{Re}[n_{\text{eff}}]}{d\lambda^2}.$$

This formula indicates that the dispersion varies rapidly in the short-wavelength region, corresponding to the high slope of the dispersion curves and slower variation in the long wavelength region, corresponding to the low slope of the dispersion curves. Thus, it can be

noticed that the dispersion curves in these cases are flatter.

Because the dispersion of PCF-B, PCF-N, and PCF-T [28] depends on the structural parameters and the wavelength, we determine the dispersion values at the 1.55 μm wavelength. When Λ equals 2.0 μm and f equals 0.3, the dispersion values of PCF-B, PCF-N and PCF-T are -7.6128 , -8.98926 , and -2.95775 ps/nm/km, respectively (Table 2). Meanwhile, the dispersion magnitudes reported for hollow-core PCFs in some projects were 10 ps/nm/km at 1.060 μm [34], 60 ps/nm/km at 0.80 μm [35], and 120 ps/nm/km at 1.060 μm [36]. In contrast, the values in our work are large because the infiltration of different liquids into the core of PCFs significantly affect the value of dispersion. Thus, the aromatic compounds filling hollow-core PCFs create flat dispersion characteristics and normal dispersion curves. This fact substantially improves the supercontinuum generation to create the ultra-flat spectrum expansion.

Table 2. Value of dispersions of the fiber with various f when Λ is 2 and 2.5 μm at a wavelength of 1.55 μm (D-B, D-N, D-T are the values of dispersion of PCF filled benzene, nitrobenzene, and toluene, respectively.)

f	D (ps/nm/km)					
	$\Lambda = 2.0 \mu\text{m}$			$\Lambda = 2.5 \mu\text{m}$		
	D-B	D-N	D-T	D-B	D-N	D-T
0.30	-7.61280	-8.98926	-2.95775	-0.46667	-8.15428	-2.23706
0.35	2.48780	4.94269	4.94935	5.88874	-3.36189	4.01279
0.40	9.09266	11.54755	13.25179	12.43357	2.06108	10.56447
0.45	18.70399	21.15888	21.47950	18.35344	6.97959	16.38819
0.50	26.80876	29.26365	31.41146	23.65029	12.27644	22.79784
0.55	35.11121	37.56610	41.10117	29.07326	17.69941	28.62156
0.60	43.83372	46.28861	50.60247	35.41056	24.03671	34.88916
0.65	52.95158	55.40647	60.31910	41.74787	30.37402	41.44084
0.70	62.46480	64.91969	69.79348	48.73152	37.35767	48.41865
0.75	72.99112	75.44601	80.39833	56.47186	45.09801	56.00014
0.80	84.13518	86.59007	91.43384	64.87430	53.50045	64.29184

3.2 Optimization of structural parameters of PCFs for supercontinuum generation

The dispersion characteristics of PCF-B, PCF-N, and PCF-T [28] with various f and Λ are analyzed in detail. The results show that the PCFs core containing aromatic compounds exhibit smaller and flatter dispersion than other hollow core structures. In addition, the dispersion characteristics of PCF-B and PCF-N are improved compared with that of PCF-T [28] with the same structural parameters. When PCFs are used for supercontinuum generation, the dispersion characteristic is the most important quantity because it not only affects the supercontinuum generation efficiency but also affects other effects, such as four-wave mixing, phase modulation, and soliton. This feature determines the expansion and flatness of the supercontinuum generation emission spectrum. Therefore, the optimal structures are based on the outstanding advantages of the dispersion properties.

In our previous research [28], two optimal fiber structures of PCF-T were selected for supercontinuum generation, and they were denoted as #I_0.3 and #I_0.35. Fig. 6a and Fig. 6b describe the dependence of effective mode area and dispersion on the wavelengths. The effective mode area value of the two fibers is small (Fig. 6a). The first structure (#I_0.3; $\Lambda = 2 \mu\text{m}$; $f = 0.3$) has all-normal dispersion characteristics. Its dispersion curve is flat and close to the zero-dispersion line. The second structure (#I_0.35; $\Lambda = 2.5 \mu\text{m}$; $f = 0.35$) has a flat dispersion curve with small dispersion absolute values. Furthermore, it has zero-dispersion wavelength values and is capable of switching between normal and anomalous dispersion modes. These two optimal structures were selected to produce coherent supercontinuum generation when femtosecond pulses were pumped [28]. The dispersion characteristics of these fibers are shown in Fig. 6.

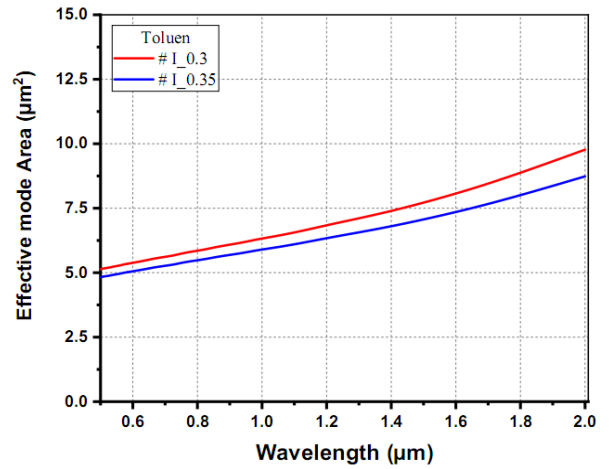


Fig. 6a. Effective mode area of PCF-Ts [28] for supercontinuum generation

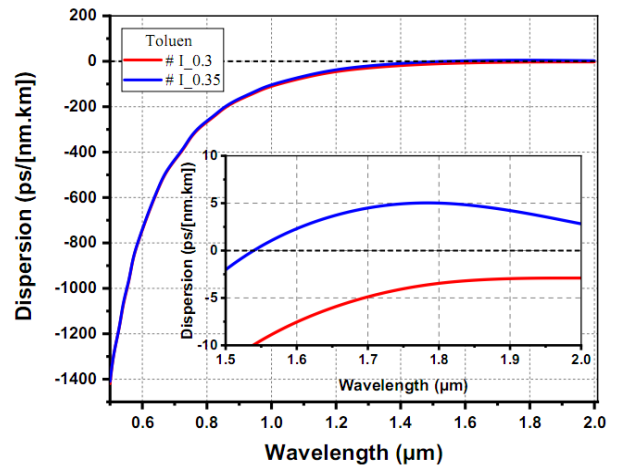


Fig. 6b. Dispersion characteristics of PCF-Ts [28] for supercontinuum generation

In this article, we compare the dispersion characteristics of PCF-B and PCF-N with that of PCF-T [28]. Based on the numerical simulations and the above results, we chose optimal PCFs with defined structural parameters for supercontinuum generation.

For PCF-Bs, three optimal structures ($\Lambda = 1.5 \mu\text{m}$, $f = 0.45$; $\Lambda = 1.5 \mu\text{m}$, $f = 0.6$ and $\Lambda = 2.5 \mu\text{m}$, $f = 0.6$) were selected, and we named them #f₁, #f₂, and #f₃, respectively. The effective mode area and dispersion characteristics of these fibers are shown in Fig. 7a and Fig. 7b. The selected fibers represent interesting dispersion characteristics required for pumped ultra-

continuous pulses with short pulses at 1.55 μm . The #f1 fiber has all-normal dispersion characteristics and a relatively small dispersion value. The relatively low filling factor ensures efficient single-mode operation. This fiber is dedicated to create coherent supercontinuum generation because of all-normal dispersion features. Unlike #f1, the #f2 and #f3 fibers exhibit anomalous dispersion features in a wide wavelength region. This property is very attractive for supercontinuum generation based on soliton separation. The #f2 fiber provides high nonlinearity because of its small effective mode area (Fig. 7a) and limited anomalous dispersion band. In contrast, the #f3 fiber has lower nonlinear coefficients (because of its larger effective mode area) and unlimited anomalous dispersion features for the long-wavelength side in the transmission range of fused silica glass.

For PCF-Ns, we identified three optimal structures and labelled them #F1, #F2, and #F3. The effective mode area and dispersion characteristics of PCF-Ns are presented in Fig. 8a and Fig. 8b. The #F1 fiber ($\Lambda = 1.0 \mu\text{m}$ and $f = 0.8$) is intended for supercontinuum generation in the anomalous dispersion mode with a pump wavelength at 1.030 μm . This fiber has a dispersion value of 33.7 ps/nm/km at the pump wavelength, and two ZDW values are observed at 960 and 1345 nm. The #F2 fiber ($\Lambda = 1.5 \mu\text{m}$ and $f = 0.4$) is expected

to emit supercontinuum generation in all-normal dispersion ranges, and its dispersion equals 2.2 ps/nm/km at the 1.56 μm pump wavelength. #F3 is labeled for the third fiber ($\Lambda = 1.5 \mu\text{m}$ and $f = 0.8$). In this case, the pump wavelength of 1.56 μm is located in the anomalous dispersion mode.

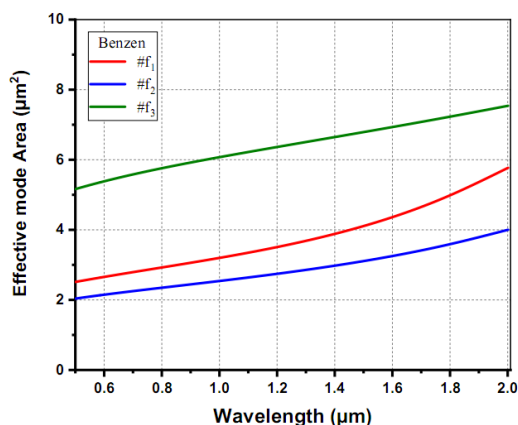


Fig. 7a. Effective mode area of PCF-Bs for supercontinuum generation

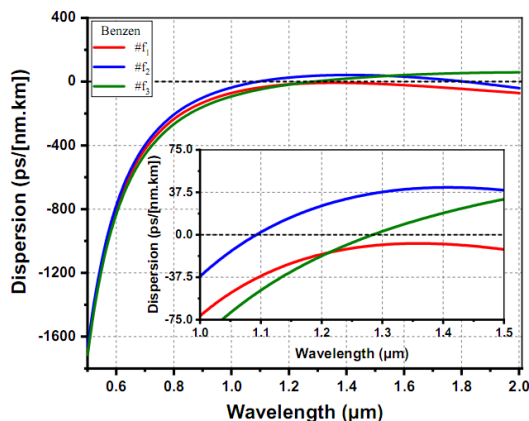


Fig. 7b. Dispersion characteristics of PCF-Bs for supercontinuum generation

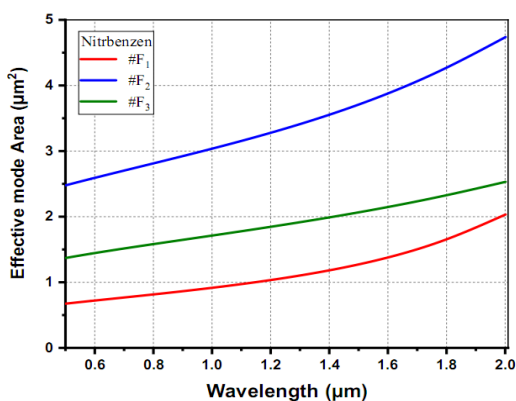


Fig. 8a. Effective mode area of PCF-Ns for supercontinuum generation

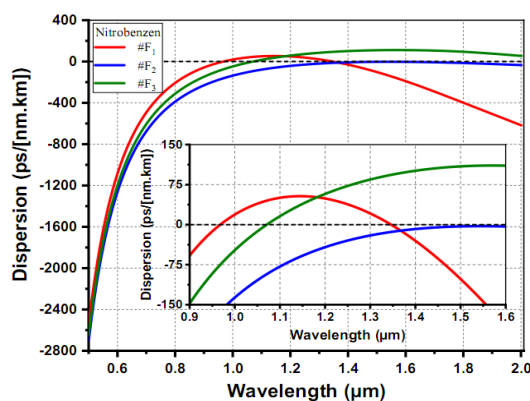


Fig. 8b. Dispersion characteristics of PCF-Ns for supercontinuum generation

The results above indicate that the values of effective mode area of optimal PCF-T [28], PCF-Bs, and PCF-Ns structures are relatively small. Compared with optimal PCF-Ts, PCF-Bs and PCF-Ns have smaller effective mode area values. This means that they have larger nonlinear coefficients, with that of PCF-Ns being the highest. Furthermore, the dispersion curves of PCF-Bs and PCF-Ns are flatter than that of PCF-Ts. Thus, these outstanding features make PCF-Bs and PCF-Ns more suitable than PCF-T [28] in a supercontinuum generation.

4 Conclusion

In this paper, we design photonic crystal fiber structures with benzene and nitrobenzene in the hollow cores. We perform 44 simulations to obtain characteristic curves of these fibers. The values of the effective mode area are relatively small, and dispersion curves are very flat and closer to the zero-dispersion line. These structures are chosen for a supercontinuum generation.

Funding statement

This research is funded by Vietnam National Foundation for Science and Technology Development (NAFOSTED) under grant number 103.03-2020.03 and Vietnam's Ministry of Education and Training (B2021- DHH-08).

References

1. Knight JC, Birks TA, Russell PSJ, and Atkin DM. All-silica single-mode optical fiber with photonic crystal cladding. *Optics Letters*. 1996;21(19):1547-9.
2. Birks TA, Knight JC, and Russell PSJ. Endlessly single-mode photonic crystal fiber. *Optics Letters*. 1997;22(13):961-3.
3. Cregan RF, Mangan BJ, Knight JC, Birks TA, Russell PSJ, Roberts PJ, et al. Single-Mode Photonic Band Gap Guidance of Light in Air. *Science*. 1999;285(5433):1537-9.
4. Philip Russell. *Photonic Crystal Fibers*. *Science*. 2003;299(5605):358-362.
5. Buczynski R, Szarniak P, Pysz D, Kujawa I, Stepień R, Szoplik T. Properties of a double-core photonic crystal fiber with a square lattice. *Proceedings of the SPIE*. 2004;5576:81-7.
6. Nascimento I, Chesini G, Sousa M, Osório J, Baptista J, Cordeiro CM, et al. Application of a photonic crystal fiber LPG for vibration monitoring. *Fifth European Workshop on Optical Fibre Sensors*. 2013;8794.
7. Barczak K. Application of Photonic Crystal Fiber in Optical Fiber Current Sensors. *Acta Physica Polonica A*. 2012;122(5):793-2.
8. Pinto AMR, Lopez-Amo M. Photonic Crystal Fibers for Sensing Applications. *Journal of Sensors* 2012;2012: 598178.
9. Knight JC, Birks TA, Russell PSJ, de Sandro JP. Properties of photonic crystal fiber and the effective index model. *Journal of the Optical Society of America A*. 1998;15(3):748-52.
10. E. Seraji F, Asghari F. Determination of Refractive Index and Confinement Losses in Photonic Crystal Fibers Using FDFD Method: A Comparative Analysis. *International Journal of Optics and Photonics*. 2009;3(1):3-7.
11. Martelli C, Canning J, Kristensen M, Grothoff N. Refractive Index Measurement within a Photonic Crystal Fibre Based on Short Wavelength Diffraction. *Sensors* 2007;7(11):2492-6.
12. Ferrando A, Silvestre E, Miret JJ, Andrés P, Andrés MV. Guiding Mechanism in Photonic Crystal Fibers. *Optics and Photonics News*. 2000;11(12):32-3.
13. Mortensen NA. Effective area of photonic crystal fibers. *Optics Express*. 2002;10(7):341-8.
14. Nagaraju N, Eliyaz M, Ksihore KLN. Dispersion and Effective Area of Air Hole Containing Photonic Crystal Fibres. *IOSR Journal of Electronics and Communication Engineering*. 2017;12(13):9-12.
15. Reeves WH, Knight JC, Russell PSJ, Roberts PJ. Demonstration of ultra-flattened dispersion in photonic crystal fibers. *Optics Express*. 2002;10(14):609-13.
16. Dabas B, Sinha RK. Dispersion characteristic of hexagonal and square lattice chalcogenide As_2Se_3

- glass photonic crystal fiber. *Optics Communications*. 2010;283(7):1331-7.
17. Karasawa N. Dispersion properties of liquid-core photonic crystal fibers. *Applied Optics*. 2012;51(21):5259-65.
 18. Olyae S, Taghipour F. A new design of photonic crystal fiber with ultra-flattened dispersion to simultaneously minimize the dispersion and confinement loss. *Journal of Physics: Conference Series*. 2011;276:012080.
 19. Pniewski J, Stefaniuk T, Van HL, Long VC, Van LC, Kasztelan R, et al. Dispersion engineering in nonlinear soft glass photonic crystal fibers infiltrated with liquids. *Applied Optics*. 2016;55(19):5033-40.
 20. Xuan KD, Van LC, Long VC, Dinh QH, Van Mai L, Trippenbach M, et al. Influence of temperature on dispersion properties of photonic crystal fibers infiltrated with water. *Optical and Quantum Electronics*. 2017;49(2):87.
 21. White TP, McPhedran RC, de Sterke CM, Botten LC, Steel MJ. Confinement losses in microstructured optical fibers. *Optics Letters*. 2001;26(21):1660-2.
 22. Tajima K, Jian Z, Nakajima K, Sato K. Ultralow loss and long length photonic crystal fiber. *Journal of Lightwave Technology*. 2004;22(1):7-10.
 23. Chen D, Shen L. Ultrahigh Birefringent Photonic Crystal Fiber with Ultralow Confinement Loss. *IEEE Photonics Technology Letters*. 2007;19(4):185-7.
 24. Koohi-Kamalia F, Ebnali-Heidarib M, Moravvej-Farshic MK. Designing a dual-core photonic crystal fiber coupler by means of microfluidic infiltration. *International Journal of Optics and Photonics*. 2012;6(2):83-96.
 25. Thenmozhi H, Mani Rajan M, Devika V, Vigneswaran D, Ayyanar N. D-glucose sensor using photonic crystal fiber. *Optik*. 2017;145:489-94.
 26. Ebnali-Heidari M, Dehghan F, Saghaei H, Koohi-Kamali F, Moravvej-Farshi MK. Dispersion engineering of photonic crystal fibers by means of fluidic infiltration. *Journal of Modern Optics*. 2012;59(16):1384-90.
 27. Liu S, Gao W, Li H, Dong Y, Zhang H. Liquid-filled simplified hollow-core photonic crystal fiber. *Optics & Laser Technology*. 2014;64:140-4.
 28. Van LC, Anuszkiewicz A, Ramaniuk A, Kasztelan R, Xuan KD, Long VC, et al. Supercontinuum generation in photonic crystal fibres with core filled with toluene. *Journal of Optics*. 2017;19(12):125604.
 29. Bozolan A, de Matos CJS, Cordeiro CMB, dos Santos EM, Travers J. Supercontinuum generation in a water-core photonic crystal fiber. *Opt Express*. 2008;16(13):9671-6.
 30. Guo Z, Yuan J, Yu C, Sang X, Wang K, Yan B, et al. Highly Coherent Supercontinuum Generation in the Normal Dispersion Liquid-Core Photonic Crystal Fiber. *Progress In Electromagnetics Research M*. 2016;48:67-76.
 31. Wang C-c, Li W-m, Li N, Wang W-q. Numerical simulation of coherent visible-to-near-infrared supercontinuum generation in the CHCl₃-filled photonic crystal fiber with 1.06 μm pump pulses. *Optics & Laser Technology*. 2017;88:215-21.
 32. Ho PP, Alfano RR. Optical Kerr effect in liquids. *Physical Review A*. 1979;20(5):2170-87.
 33. Couris S, Renard M, Faucher O, Lavorel B, Chauv R, Koudoumas E, et al. An experimental investigation of the nonlinear refractive index (n₂) of carbon disulfide and toluene by spectral shearing interferometry and z-scan techniques. *Chemical Physics Letters*. 2003;369(3-4):318-24.
 34. Lim H, Wise FW. Control of dispersion in a femtosecond ytterbium laser by use of hollow-core photonic bandgap fiber. *Optics Express*. 2004;12(10):2231-5.
 35. Engelbrecht CJ, Johnston RS, Seibel EJ, Helmchen F. Ultra-compact fiber-optic two-photon microscope for functional fluorescence imaging in vivo. *Optics Express*. 2008;16(8):5556-64.
 36. Wan B, Zhu L, Ma X, Li T, Zhang J. Characteristic Analysis and Structural Design of Hollow-Core Photonic Crystal Fibers with Band Gap Cladding Structures. *Sensors*. 2021;21(1):284.